

## **Multibody interactions of floating bodies with time domain predictions**

KARA, Fuat

Available from Sheffield Hallam University Research Archive (SHURA) at:

<http://shura.shu.ac.uk/25889/>

---

This document is the author deposited version. You are advised to consult the publisher's version if you wish to cite from it.

### **Published version**

KARA, Fuat (2020). Multibody interactions of floating bodies with time domain predictions. Journal of Waterway, Port, Coastal and Ocean Engineering.

---

### **Copyright and re-use policy**

See <http://shura.shu.ac.uk/information.html>

# Multibody interactions of floating bodies with time domain predictions

Fuat Kara

Sheffield Hallam University, S1 1WB, UK

e-mail: [fuat.kara@shu.ac.uk](mailto:fuat.kara@shu.ac.uk)

## Abstract

The applications of the three-dimensional transient panel code ITU-WAVE based on potential theory is further extended to take into account the multibody interactions in an array system using linear and square arrays. The transient wave-body interactions of first-order radiation and diffraction hydrodynamic parameters are solved as the impulsive velocity potential to predict Impulse Response Functions (IRFs) for each mode of motion. It is shown that hydrodynamic interactions are stronger when the bodies in an array system are close proximity and these hydrodynamic interactions are reduced considerably and shifted to larger times when the separation distances are increased. The numerical predictions of radiation (added-mass and damping coefficients) and exciting (diffraction and Froude-Krylov) forces are presented on each floating bodies in an array system and on single structure considering array as single floating body. Furthermore, the numerical experiment shows the hydrodynamic interactions are more pronounced in the resonant frequency region which are of important for fluid forces over bodies, responses and designs of multibody floating systems. The present numerical results of ITU-WAVE are validated against analytical, other numerical and experimental results for single body, linear arrays (two, five and nine floating bodies) and square arrays of four truncated vertical cylinders.

**Keywords:** multibody interaction; transient free-surface Green function; boundary integral equation; impulse response functions, response amplitude operators; free decay motion.

## 1. Introduction

The hydrodynamic interactions play significant role related to hydrodynamic loads, motions and responses over each multibody when the separation distance between floating bodies in an array system are close proximity. There are wide ranges of application of hydrodynamic interactions in practice including wave energy converter and floating offshore wind turbines arrays, floating airports and bridges supported with multiple columns, catamarans and other multi-hull floating vessels, marine operation related to replenishment of two floating vessels. The oscillation of each body radiates waves assuming that other bodies are not present. Some of these radiated waves, which can be considered as incident waves, interact with the bodies of the array causing diffraction phenomena while others radiate to infinity.

The hydrodynamic interactions was predicted with the point absorber approximation [1] in which the response amplitude are considered as equal for all devices. Moreover, the characteristic dimensions

(e.g. diameter) of the devices are considered small in terms of incident wave length. This approximation implicitly means that wave diffraction is not significant and can be ignored [2]. The diffraction limitation of the point absorber prediction was overcome with plane wave analysis in which interactions of diverging waves considered as plane waves between floating bodies in arrays are taken into account while the near-field waves (or evanescent waves) effects are ignored. This implies that separation distance between devices is large relative to wavelength [3-5]. The restriction on separation distance between devices or exclusion of near-field waves was included with multiple scattering methods in which the superposition of incident wave potential, diverging and near-field waves, and radiated waves by the oscillation of devices are taken into account. In this way, the wave field around floating bodies can be represented accurately [6-8]. As the accurate solution requires high number of diffracted and radiated wave superposition with iteration, this process increases the computational time significantly [9].

The restriction on the computational time was avoided by the use of the direct matrix method in which the multiple scattering prediction are combined with a direct approximation [10] and unknown wave amplitudes are predicted simultaneously rather than iteratively. As the numerical results of this approach, which is exact depending on infinite summation truncation, were very accurate compared to other numerical approximations, this method was applied to many different engineering problems including near trapping problem in large arrays [10], very large floating structures [11,12], tension-leg-platforms [13], wave energy converters [14].

If the geometry of the bodies in an array system can be defined analytically, the above exact formulations can be used. However, in the case of arbitrary geometries, these approximations cannot be used. As a next step, the numerical methods to predict hydrodynamic interactions for multi-bodies are studied extensively by many researchers including [15] who used the strip theory in which the hydrodynamic interactions are considered as two-dimensional flow. The unified theory was used to overcome the low frequency limitations of strip theory [16,17]. These two-dimensional approaches give poor predictions as the hydrodynamic interactions including separation distances between the bodies are neglected in the calculations.

As the hydrodynamic interactions are inherently three-dimensional and three-dimensional effects play a significant role in the dissipation of wave energy between bodies, three-dimensional numerical approximations need to be used for accurate prediction of the wave loads and motions over array systems. The hydrodynamic interaction effects are automatically taken into account as each discretized panel has its influence on all other panels in three-dimensional numerical models. The viscous Computational Fluid Dynamics (CFD) methods for full fluid domain or viscous CFD in the near field and inviscid CFD in the far field can be used for the prediction of three-dimensional non-linear flow field due to incident waves. However, the required computational time to solve these kinds of problems is not suited for practical purposes yet [18].

An alternative approach to a viscous solution is the three-dimensional potential flow approximation to solve the hydrodynamic interactions. The computational time of potential approximation which neglect

the viscous effect is much less than viscous CFD and are used to predict the hydrodynamic loads over floating single body and arrays. The prediction of three-dimensional hydrodynamic interaction effects on arrays can be obtained using three-dimensional frequency or time domain approaches and two popular approximations were used for this purpose. These are Green's function formulation [19-21] and Rankine type source distribution [22-24]. The Green function's approach satisfies the free surface boundary condition and condition at infinity automatically, and only the body surface needs to be discretized with panels, while the source and dipole singularities are distributed discretizing both the body surface and a portion of the free surface in Rankine type approximation. The requirement of the discretization of some portion of the free surface in order to satisfy the condition at infinity using panels increases the computational time considerably.

One of the topics that extensively studied related to hydrodynamic interactions of multibodies is the wave trapping and near trapping which increase the magnitude of the hydrodynamic loads at certain wave numbers significantly. The wave trapping, in which all wave energy is captured in the gap and no energy dissipated to infinity at critical wave numbers, occurs due to hydrodynamic interaction of scattered waves in an infinite number of array systems [25, 26]. In the case of finite number of arrays, near-trapping, in which only small amount of energy in the gap radiated to infinity, occurs even with small number of floating bodies including four legs of tension leg platforms, five or nine linear arrays. The multibody interaction due to oscillation of floating bodies in the array changes the behaviour of the added-mass and damping coefficients significantly over the range of wave frequencies especially around resonant frequency which are very important for the response and motion of the floating bodies in an array system [13,27,28]. The hydrodynamic interactions due to radiation also contribute the exciting forces significantly. It is also important to know multibody interactions for the performance of wave energy converter arrays as the hydrodynamic interaction could increase or decrease absorbed power depending on separation distance and heading angles [29]. The wave trapping increases the performance and efficiency of the wave energy converters as more energy would be available to capture in the case of the trapped wave conditions.

In the present paper, the time dependent hydrodynamic radiation and exciting forces' IRFs (which are used for the time marching of the equation of motion in order to find displacement, velocity, and acceleration of each body in an array system) are predicted by the use of the transient free-surface wave Green function [19,29-37]. The IRFs, free-decay motion, radiation (added-mass and damping) coefficients, exciting force amplitudes and RAOs of the present ITU-WAVE numerical results for single body, linear array and square array systems will be validated against analytical, other numerical and experimental results.

## 2. Equation of motion of multibodies

A right-handed coordinate system is used to define the fluid action and a Cartesian coordinate system  $\vec{x} = (x, y, z)$  is fixed to the body which is used for the solution of the linearized problem in the time domain Fig. 1. Positive x-direction is towards the forward, positive z-direction points upwards, and the  $z=0$  plane (or  $xy$ -plane) is coincident with calm water. The bodies undergo oscillatory motion about their

mean positions due to incident wave field. The origin of the body-fixed coordinate system  $\vec{x} = (x, y, z)$  is located at the centre of the xy-plane. The solution domain consists of the fluid bounded by the free surface  $S_f(t)$ , the body surface  $S_b(t)$ , interaction between body and free surfaces  $\Gamma$  and the boundary surface at infinity  $S_\infty$  Fig. 1 [19] where  $\beta$  incident wave angle, numbers represents the position of each multibody in array system, d separation distance between body centres.

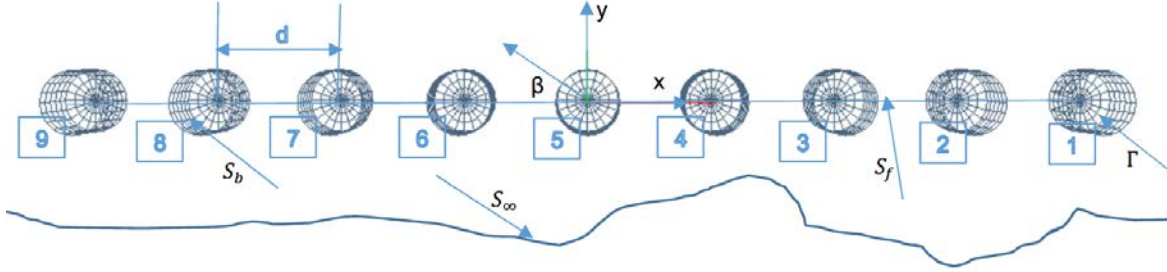


Fig. 1: Coordinate system and surface of nine (1x9) multibodies in a linear array system

The following assumptions are taken into account in order to solve the physical problem. If the fluid is unbounded (except for the submerged portion of the body on the free surface), ideal (inviscid and incompressible), and its flow is irrotational (no fluid separation and lifting effect), the principle of mass conservation dictates the total disturbance velocity potential  $\Phi(\vec{x}, t)$ . This velocity potential is harmonic and governed by Laplace equation everywhere in the fluid domain as  $\nabla^2 \Phi(\vec{x}, t) = 0$  and the disturbance flow velocity field  $\vec{V}(\vec{x}, t)$  may then be described as the gradient of the potential  $\Phi(\vec{x}, t)$  (e.g.  $\vec{V}(\vec{x}, t) = \nabla \Phi(\vec{x}, t)$ ).

The dynamics of a floating body's unsteady oscillations are governed by a balance between the inertia of the floating body and the external forces acting upon it. This balance is complicated by the existence of radiated waves which results from the oscillations of the bodies and the scattering of the incident waves. This means that waves generated by the floating bodies at any given time will persist indefinitely and the waves of all frequencies will be generated on the free surface. These generated waves, in principle, affect the fluid pressure field and hence the body force of the floating bodies at all subsequent times. This situation introduces memory effects and is described mathematically by a convolution integral. Having assumed that the system is linear, the equation of motion of any floating bodies may be written in a form [38]

$$\sum_{k=1}^6 (M_{kk_i} + a_{kk_i}) \ddot{x}_{k_i}(t) + (b_{kk_i}) \dot{x}_{k_i}(t) + (C_{kk_i} + c_{kk_i}) x_{k_i}(t) + \int_0^t d\tau K_{kk_i}(t - \tau) \dot{x}_{k_i}(\tau) = \int_{-\infty}^{\infty} d\tau K_{kD_i}(t - \tau) \zeta(\tau) \quad (1)$$

where  $i = 1, 2, 3, \dots, N$  is the N number of body in the array systems.  $k = 1, 2, 3, \dots, 6$  represents six-rigid body modes of surge, sway, heave, roll, pitch and yaw, respectively. The displacement of the floating bodies from its mean position in each of its rigid-body modes of motion is given  $x_k(t) = (1, 2, 3, \dots, N)^T$ ,

and the over-dots indicates differentiation with respect to time.  $\ddot{x}_k(t)$  and  $\dot{x}_k(t)$  are acceleration and velocity, respectively.  $M_{kk}$  inertia matrix of the floating body and  $C_{kk}$  linearized hydrostatic restoring force coefficients. As the same floating body is used in the array, the elements of both mass and restoring coefficients equal to each other for each body  $m_1 = m_2 = \dots = m_N = m$  and  $C_1 = C_2 = \dots = C_N = C$ , respectively.  $m$  and  $C$  are the mass and restoring coefficient for single body, respectively.

$$M_{kk} = \begin{pmatrix} m_1 & \dots & 0 \\ \vdots & \ddots & \vdots \\ 0 & \dots & m_N \end{pmatrix} \quad C_{kk} = \begin{pmatrix} C_1 & \dots & 0 \\ \vdots & \ddots & \vdots \\ 0 & \dots & C_N \end{pmatrix} \quad (2)$$

The coefficients of  $a_{kk}$ ,  $b_{kk}$  and  $c_{kk}$  in Eq. (1) account for the instantaneous forces proportional to the acceleration, velocity and displacement, respectively. The coefficients  $a_{kk}$ ,  $b_{kk}$  and  $c_{kk}$  are also the time and frequency independent constants which depend on the body geometry and is related to added mass, damping and hydrostatic restoring coefficients, respectively.

The radiation Impulse Response Functions (IRFs)  $K_{kk}(t)$  in left-hand side of Eq. (1) is the force on the  $k$ -th body due to an impulsive velocity of the  $k$ -th body. The memory function  $K_{kk}(t)$  accounts for the free surface effects which persist after the motion occurs. The term 'memory function' for the radiation problem is used to distinguish this portion of IRFs from the instantaneous force components outside of the convolution on the left-hand side of Eq. (1). The memory coefficient  $K_{kk}(t)$  is the time dependent part and depends on body geometry and time. It contains the memory (or transient) effects of the fluid response. The convolution integral on the left-hand side of Eq. (1), whose kernel is a product of the radiation IRFs  $K_{kk}(t)$  and velocity of the floating body  $\dot{x}_k(t)$ , is a consequence of the radiated wave of the floating body. When this wave is generated, it affects the floating body at each successive time step [39].

$$K_{kk}(t) = \begin{pmatrix} K_{11} & \dots & K_{1N} \\ \vdots & \ddots & \vdots \\ K_{N1} & \dots & K_{NN} \end{pmatrix}, a_{kk} = \begin{pmatrix} a_{11} & \dots & a_{1N} \\ \vdots & \ddots & \vdots \\ a_{N1} & \dots & a_{NN} \end{pmatrix}, b_{kk} = \begin{pmatrix} b_{11} & \dots & b_{1N} \\ \vdots & \ddots & \vdots \\ b_{N1} & \dots & b_{NN} \end{pmatrix}, c_{kk} = \begin{pmatrix} c_{11} & \dots & c_{1N} \\ \vdots & \ddots & \vdots \\ c_{N1} & \dots & c_{NN} \end{pmatrix} \quad (3)$$

The diagonal terms in Eq. (3) represent the each floating body's  $K_{kk}(t)$ ,  $a_{kk}$ ,  $b_{kk}$  and  $c_{kk}$  whilst off-diagonal terms represent the interactions of each body with other floating bodies in the array systems.

The term  $K_{kD}(t) = (K_{1D}, K_{2D}, K_{3D}, \dots, K_{ND})^T$  on the right-hand side of Eq. (1) are the components of the exciting force and moment's IRFs including Froude-Krylov and diffraction due to the incident wave elevation  $\zeta(t)$  which is the arbitrary wave elevation and defined at the origin of the coordinate system of Fig. 1 in the body-fixed coordinate system. The kernel  $K_{kD}(t)$  represents the force on the  $k$ -th body due to a uni-directional impulsive wave elevation with a heading angle of  $\beta$  [20].

Once the restoring matrix, inertia matrix and fluid forces e.g. radiation and diffraction force IRFs are known, the equation of motion of multibody floating system Eq. (1) may be time marched using the fourth-order Runge-Kutta method [19,29-37].

### 3. Integral equation of multibodies

The initial boundary value problem consisting of initial condition, free surface and body boundary condition may be represented as an integral equation using a transient free-surface Green's function [40]. Applying Green's theorem over the transient free-surface Green function derives the integral equation. Integrating Green's theorem in terms of time from  $-\infty$  to  $+\infty$  using the properties of transient free-surface Green's function and potential theory, the integral equation for the source strength on each multibody may be written as in [19].

$$\begin{cases} \sigma_1(P, t) + \frac{1}{2\pi} \iint_{S_1} dS_Q \frac{\partial}{\partial n_P} G(P, Q, t - \tau)|_{S_1} \sigma_1(Q, t) + \dots + \frac{1}{2\pi} \iint_{S_N} dS_Q \frac{\partial}{\partial n_P} G(P, Q, t - \tau)|_{S_1} \sigma_N(Q, t) = -2 \frac{\partial}{\partial n_P} \phi(P, t)|_{S_1} \\ \vdots \\ \sigma_N(P, t) + \frac{1}{2\pi} \iint_{S_1} dS_Q \frac{\partial}{\partial n_P} G(P, Q, t - \tau)|_{S_N} \sigma_1(Q, t) + \dots + \frac{1}{2\pi} \iint_{S_N} dS_Q \frac{\partial}{\partial n_P} G(P, Q, t - \tau)|_{S_N} \sigma_N(Q, t) = -2 \frac{\partial}{\partial n_P} \phi(P, t)|_{S_N} \end{cases} \quad (4)$$

And potential on each multibody

$$\begin{cases} \phi_1(P, t) = -\frac{1}{4\pi} \iint_{S_1} dS_Q G(P, Q, t - \tau)|_{S_1} \sigma_1(Q, t) - \dots - \frac{1}{4\pi} \iint_{S_N} dS_Q G(P, Q, t - \tau)|_{S_1} \sigma_N(Q, t) \\ \vdots \\ \phi_N(P, t) = -\frac{1}{4\pi} \iint_{S_1} dS_Q G(P, Q, t - \tau)|_{S_N} \sigma_1(Q, t) - \dots - \frac{1}{4\pi} \iint_{S_N} dS_Q G(P, Q, t - \tau)|_{S_N} \sigma_N(Q, t) \end{cases} \quad (5)$$

$G(P, Q, t, t - \tau) = \left(\frac{1}{r} - \frac{1}{r'}\right) \delta(t - \tau) + H(t - \tau) \tilde{G}(P, Q, t - \tau)$  is the Green function in which the first term  $\left(\frac{1}{r} - \frac{1}{r'}\right)$  represents Rankine term and second term  $\tilde{G}(P, Q, t - \tau)$  represents the memory (or transient) part of the transient free-surface Green function of the source potential.  $r = \sqrt{(x - \xi)^2 + (y - \eta)^2 + (z - \zeta)^2}$  the distance between field and source point,  $r' = \sqrt{(x - \xi)^2 + (y - \eta)^2 + (z + \zeta)^2}$  the distance between field point and image point over free surface.  $\delta(t - \tau)$  is Dirac delta function.  $H(t - \tau)$  is Heaviside unit step function. The evaluation of the Rankine source type terms  $(1/r, 1/r')$  is analytically integrated over quadrilateral panels using the method and formulas of [41]. For small values of  $r$ , exact solution is used for the surface integration. For intermediate values of  $r$ , a multi-pole expansion is used whilst for large values of  $r$ , a simple monopole expansion is used.

The transient part of Green function is given as  $\tilde{G}(P, Q, t - \tau) = 2 \int_0^\infty dk \sqrt{kg} \sin(\sqrt{kg}(t - \tau)) e^{k(z+\zeta)} J_0(kR)$  where  $J_0$  the Bessel function of zero order. The Green function  $\tilde{G}(P, Q, t, \tau)$  represents the potential at the field point  $P(x(t), y(t), z(t))$  and time  $t$  due to an impulsive disturbance at source point  $Q(\xi(t), \eta(t), \zeta(t))$  and time  $\tau$ . The surface integrals over each quadrilateral element involving the wave term of the transient free surface Green function  $\tilde{G}(P, Q, t - \tau)$  are solved analytically [19-21] and then integrated numerically using a coordinate mapping onto a standard region and Gaussian quadrature. For surface elements, the arbitrary quadrilateral element is first mapped into a unit square. A two-dimensional Gaussian quadrature

formula of any desired order is then used to numerically evaluate the integral. The evaluation of the memory part  $\tilde{G}(P, Q, t - \tau)$  of the transient free surface Green function and its derivatives with efficient and accurate methods is one of the most important elements in this problem. Depending on the values of  $P, Q, t$  five different methods are used to evaluate  $\tilde{G}(P, Q, t - \tau)$ ; power series expansion, an asymptotic expansion, Filon integration, Bessel function and asymptotic expansion of complex error function.

The integral equation for the source strength Eq. (4) is first solved, and then this source strength is used in the potential formulation Eq. (5) to find potential and fluid velocities at any point in the fluid domain. The time marching scheme is used for the solution of the integral equation Eq. (4). The form of the equation is consistent for both the radiation and the diffraction potentials so that the same approach may be used for all potentials. Since the transient free surface Green function  $\tilde{G}(P, Q, t - \tau)$  satisfies free surface boundary condition and condition at infinity automatically, in this case only the underwater surface of the multibodies needs to be discretized using quadrilateral/triangular elements. The resultant boundary integral equation Eq. (4) is discretized using panels over which the value of the source strength is assumed to be constant and solved using the trapezoidal rule to integrate the memory or convolution part in time. This discretization reduces the continuous singularity distribution to a finite number of unknown source strengths. The integral equation Eq. (4) are satisfied at collocation points located at the null points of each panel. This gives a system of algebraic equations which are solved for the unknown source strengths. At each time step the new value of the source strength is determined on each quadrilateral panel.

#### **4. ITU-WAVE transient wave-structure interaction computational code**

The hydrodynamics functions and coefficients in the present paper are predicted with in-house ITU-WAVE three-dimensional direct time domain numerical code. ITU-WAVE transient wave-structure interaction code which is coded using C++ was validated against experimental, analytical, and other published numerical results [19,29-37] and used to predict the seakeeping characteristics (e.g. radiation and diffraction), response of floating systems, ship resistance, ship added-resistance, hydroelasticity of the floating bodies, wave power absorption from ocean waves with single and multibody floating systems using latching control.

#### **5. Numerical results**

The present ITU-WAVE numerical results are compared with the analytical, other numerical and experimental results of two, five, nine linear arrays, square array and single sphere in order to validate the present numerical predictions for hydrodynamic interactions and response of multibody systems.

##### **5.1. Two (1x2) truncated vertical cylinder arrays**



Two truncated vertical cylinders are considered as a single unit (or mass, structure) and individual mass for the present numerical predictions which are compared with existing analytical and other numerical results for validation purposes.

#### 5.1.1. Two (1x2) truncated vertical cylinder arrays as a single mass

Two truncated vertical cylinders Fig. 2 is used for numerical analysis as a single mass. It is assumed two cylinders have the same draught and radius although present method can be applied for different draught and radius. The truncated cylinders have the radius  $R$ , draught  $2R$  and hull separation between body centres  $d=2.6R$ . It is assumed that two truncated cylinders are free for surge mode and fixed for other modes. These two truncated cylinders are studied to predict surge radiation and exciting IRFs in time and added-mass, damping coefficients and exciting force amplitudes in frequency domain. The time domain and frequency domain results are related to each other through Fourier transforms in the context of linear analysis. The present ITU-WAVE numerical results for surge added-mass and damping coefficients and exciting force amplitudes (which are the sum of the diffraction and Froude-Krylov forces) with heading angle  $\beta = 180^\circ$  are compared with the analytical results of [10].

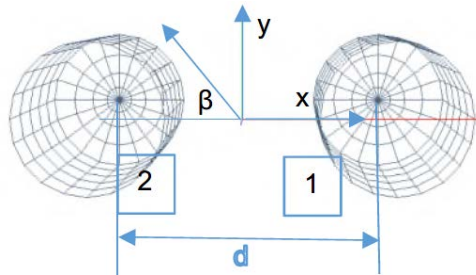


Fig. 2: Two (1x2) truncated vertical cylinders with hull separation distance between body centres  $d = 2.6R$

Fig. 3 shows the radiation IRF for surge mode. As two truncated vertical cylinders are symmetric in terms of  $xz$ -coordinate plane of the reference coordinate system, only single hull form is discretized for numerical analysis. Numerical experience showed that numerical results are not very sensitive in terms of non-dimensional time step size  $t\sqrt{g/R}$  (where  $t$  is time,  $g$  gravitational acceleration,  $R$  radius) of 0.01, 0.03, and 0.05 over the range of panel numbers of 128, 200, 288 on single body of two truncated vertical cylinders whilst the numerical experience also showed that the numerical results are quite sensitive in terms of panel numbers and the results at panel number 200 on single hull form is converged and used for the present ITU-WAVE numerical calculations for both two and single truncated vertical cylinder with non-dimensional time step size of 0.05.

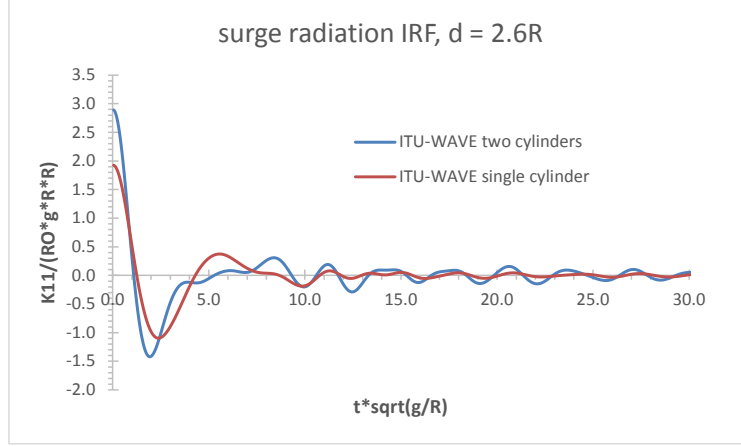


Fig. 3: Two truncated vertical cylinders as a single mass - non-dimensional surge radiation  $K_{11}(t)$  IRF at separation distance between body centres  $d = 2.6R$  and head seas  $\beta = 180^\circ$

The time dependent radiation IRFs in time domain are related to the frequency dependent added-mass and damping coefficients in frequency domain through Fourier transforms when the motion is considered as a time harmonic motion. Added-mass  $A_{11}(\omega)$  and damping coefficients  $B_{11}(\omega)$  in Fig. 4 is obtained by the Fourier transform of surge radiation IRF  $K_{11}(t)$  of Fig. 3.

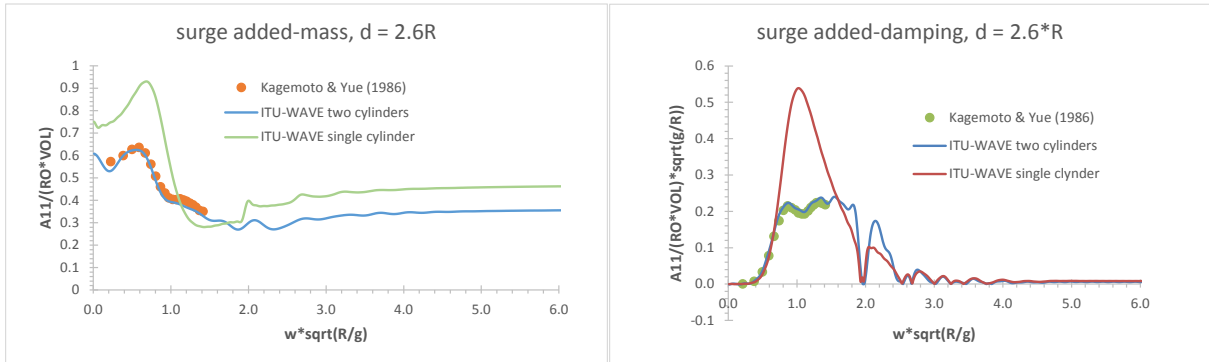
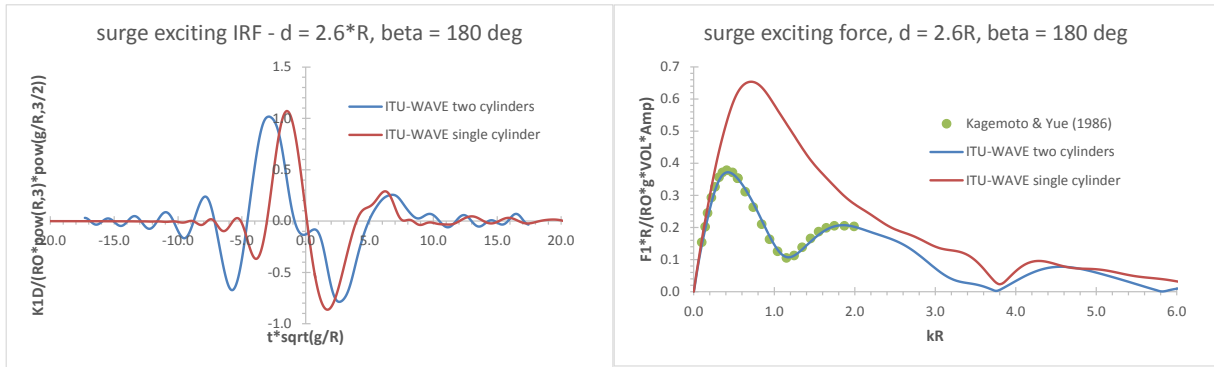


Fig. 4: Two truncated vertical cylinders as a single mass - non-dimensional surge added-mass and damping coefficients at separation distance between body centres  $d = 2.6R$ .

ITU-WAVE numerical results of added-mass and damping coefficients in surge mode of two cylinders are in satisfactory agreement with the analytical prediction [10] as can be seen in Fig. 4. In addition, the added mass and damping coefficients of the two cylinder array are presented in Fig. 4 and compared to those from the single cylinders. It can be seen in Fig. 4 that the behaviours of two cylinders results in surge mode are significantly different from those of single cylinder due to trapped waves and hydrodynamic interactions in the gap of two cylinders.

As in radiation force analysis, the time dependent exciting IRFs in time domain are related to the frequency dependent force amplitude in frequency domain via Fourier transforms when the motion is considered as a time harmonic motion. The exciting force amplitudes  $F_1(\omega)$  in Fig. 5 (right) is obtained by Fourier transform of surge exciting IRF  $K_{10}(t)$  of Fig. 5 (left).

322



323

324

325

326

327

328

329

330

331

332

333

334

335

336

337

338

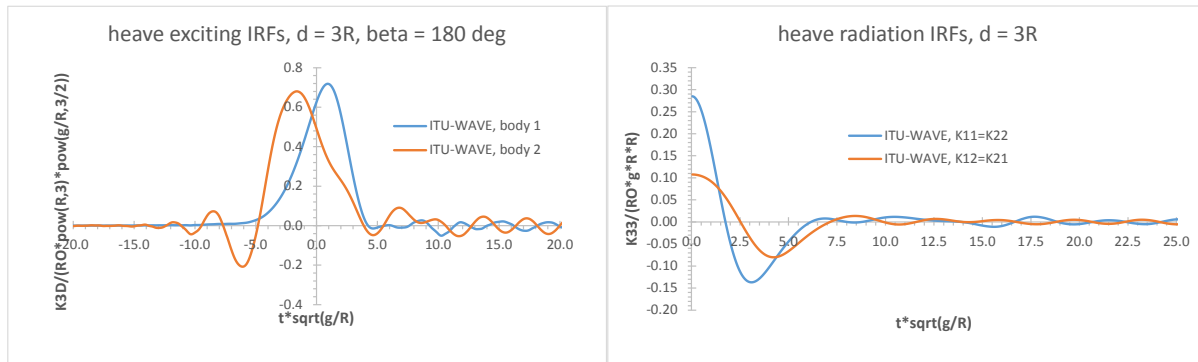
339

Fig. 5: Two truncated vertical cylinders as a single mass - non-dimensional surge exciting IRF and force amplitude at separation distance between body centres  $d = 2.6R$  and head seas  $\beta = 180^\circ$ .

The effects of diffraction hydrodynamic interactions in surge mode are effective in the whole frequency range as can be observed in Fig. 5. This interaction effects in surge mode are even stronger in a limited frequency range which is of interest for the motions of the bodies in array systems and is around  $kR = 0.5$  and  $kR = 2.0$  of non-dimensional frequency in radiation and diffraction surge mode in Fig. 4 and Fig. 5, respectively.

#### 5.1.2. Two (1x2) truncated vertical cylinder arrays as an individual mass

The truncated cylinders have the radius  $R$ , draught  $R/2$  and hull separation between centre of the bodies  $d = 3R, 5R$ . It is assumed that two truncated cylinders are free in heave mode and fixed for other modes. These two truncated cylinders are studied to predict heave radiation and diffraction IRFs Fig. 6 in time and added-mass, damping coefficients and exciting force amplitudes in frequency domain.



340

341

342

343

344

345

346

Fig.6: Two (1x2) truncated vertical cylinders as an individual mass - non-dimensional heave exciting (left) and radiation (left) IRFs at separation distance between body centres  $d = 3R$  of Fig. 2.

Numerical experience showed that present predicted results at panel number 200 for each body is converged and used for the present ITU-WAVE numerical calculations with non-dimensional time step size of 0.05. It may be noticed from Fig. 6 (left) as expected body 1 interacts with the incident wave first

and the interaction of body 2 with incident wave which is in the wake of body 1 is delayed in the case of heading angle  $\beta = 180^\circ$ .

The radiation IRFs for heave mode in the case of two interacting bodies for each body in arrays are presented in Fig. 6 (right). The radiation IRFs  $K_{12}(t)$  which represents the interactions between two truncated vertical cylinders is very strong and the same order with  $K_{11}(t)$ . The interaction IRFs on body 1 and body 2 have the same magnitude and sign as it is presented in Fig. 6. This implies that giving one body an impulsive velocity in one mode causes a force in the same mode on the other body after some finite time  $t$ , which is the time it takes the wave to move the distance between bodies. This means that energy is trapped in the gap between bodies, only a minor part of the energy is radiated outwards each time the wave is reflected off the body.

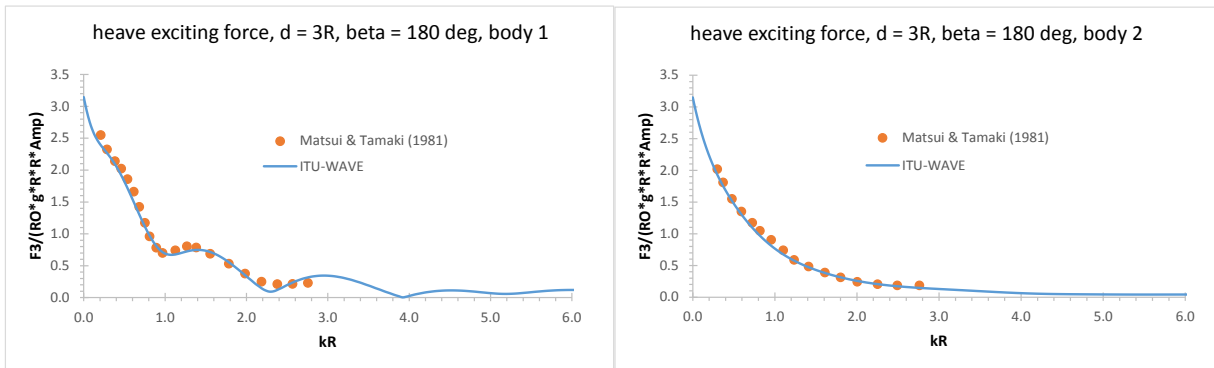
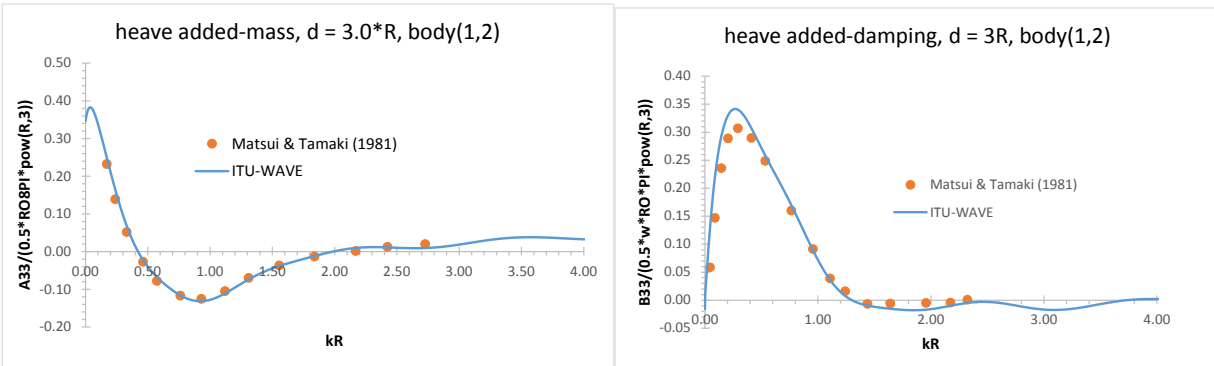


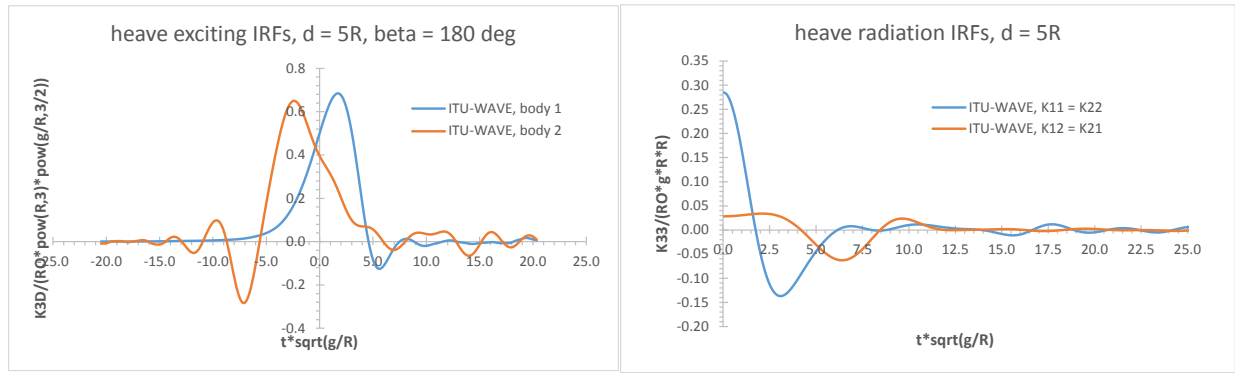
Fig.7: Two (1x2) truncated vertical cylinders as an individual mass - non-dimensional exciting force amplitude for body 1 and body 2 at separation distance between body centres  $d = 3R$  and heading angle 180 degrees.

Fig. 7 shows the exciting force amplitude for body 1 and body 2 for the separation distance  $d = 3R$  and heading angle 180 degrees. Fig. 7 is obtained by the Fourier transform of Fig.6 (left). It may be noticed from Fig. 7 that body 1 which interacts with the incident wave first is significantly affected due to the reflection of the waves by body 2. The present ITU-WAVE numerical results of exciting force amplitudes for body 1 and body 2 are compared with that of [27] which shows satisfactory agreement.



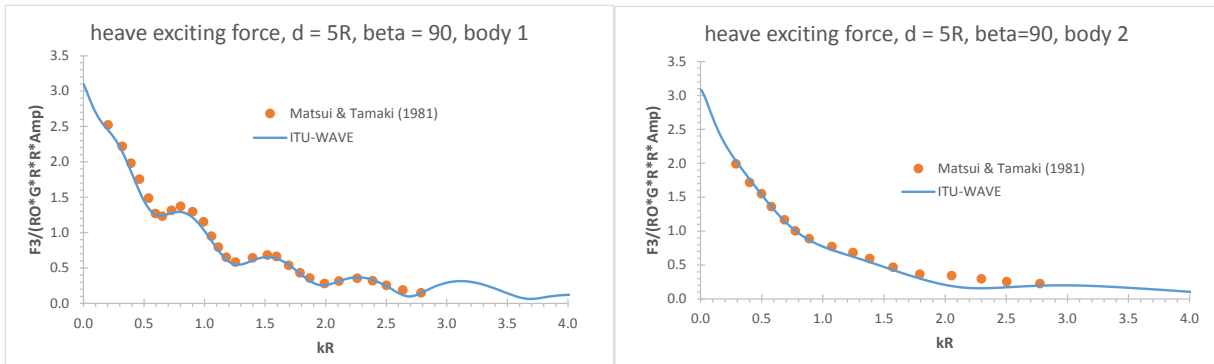
**Fig. 8:** Two (1x2) truncated vertical cylinders as an individual mass - non-dimensional heave radiation added-mass and damping coefficients at separation distance between body centres  $d = 3R$ , body(1,2) represents interaction of first and second body.

Fig. 8 shows the radiation interaction forces (added-mass and damping coefficients) for body 1 and body 2 for the separation distance  $d = 3R$ . Fig. 8 is obtained by the Fourier transform of Fig.6 (right). It may be noticed from Fig. 8 that both added-mass and damping coefficients have negative values at certain non-dimensional incident wave frequencies which is mainly due to hydrodynamic interactions of the body 1 and body 2. The present ITU-WAVE numerical results of added-mass and damping coefficients for body 1 and body 2 are compared with that of [27] which shows satisfactory agreement.



**Fig. 9:** Two (1x2) truncated vertical cylinders as an individual mass - non-dimensional heave exciting (left) and radiation (right) IRFs at separation distance between body centres  $d = 5R$  of Fig. 2.

Fig.9 shows exciting (left) heave IFRs for body 1 and body 2 and radiation (right) heave reaction (K11) and interaction (K12) IRFs. When two separation  $3R$  and  $5R$  exciting and radiation results are compared in Fig. 6 and Fig. 9, the magnitude of the exciting forces are quite similar whilst the radiation interaction IRFs are quite different. As can be seen in the left of Fig. 6 and Fig. 9, the magnitude of Fig. 9 is much smaller compared to that of Fig. 6 due to the increase of separation distance between individual bodies.



**Fig. 10:** Two (1x2) truncated vertical cylinders as an individual mass - non-dimensional heave exciting forces for body 1 and body 2 at separation distance between body centres  $d = 5R$  and heading angle 180 degrees.

Fig. 10 shows heave exciting force amplitudes for body 1 and body 2 at separation distance  $d = 5R$  and heading angle 180 degrees. Fig. 10 is obtained by the Fourier transform of Fig.9 (left). The present

results of ITU-WAVE show satisfactory agreement with [27]. As in separation distance  $d = 3R$ , the effect of interaction for body 1 compared to body 2 is much more significant and irregular.

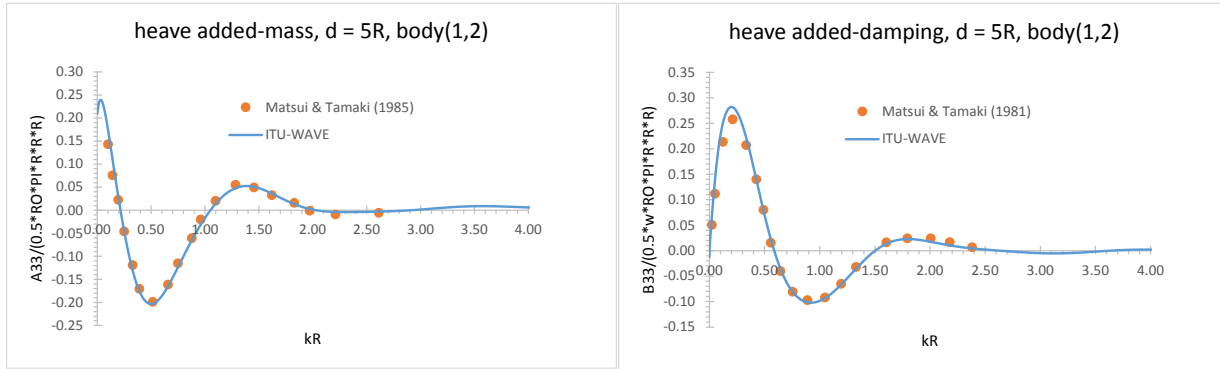


**Fig. 11:** Two (1x2) truncated vertical cylinders as an individual mass - non-dimensional heave radiation added-mass and damping coefficients at separation distance between body centres  $d = 5R$ , body(1,2) represents interaction of first and second body.

Fig. 11 shows radiation heave added-mass and damping interaction coefficients between body 1 and body 2 at separation distance  $d = 5R$ . The comparison of the present ITU-WAVE results with other numerical results [27] has acceptable agreement. When the results of added-mass and damping coefficients at separation distances of  $3R$  and  $5R$  are compared, it can be seen in Figs. 8 and Fig. 11 that coefficients have increased degree of negative values at separation distance  $d=5R$ . These are due mainly to amplitude of IRFs which are smaller than that of separation distance  $3R$ .

## 5.2. Four (2x2) truncated vertical cylinder arrays as a single mass

As in two vertical cylinder, four vertical cylinders are considered as a single mass and an individual mass in the present investigation and compared with existing analytical results [10,42].

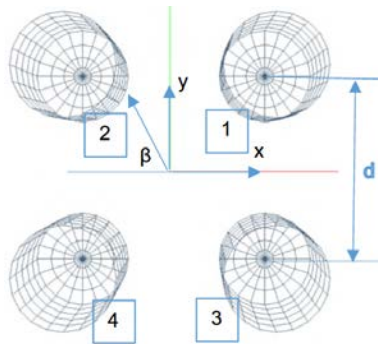


**Fig. 12:** Four (2x2) truncated vertical cylinders with hull separation distance between body centres  $d = 4R$

### 5.2.1. Four (2x2) truncated vertical cylinder arrays as an single mass

Four truncated vertical cylinder Fig. 12 is used for numerical analysis as a single mass. As in two cylinders, it is assumed that four cylinders have the same draught and radius. Four truncated cylinders

have the radius  $R$  and draught  $2R$  and hull separation between body centres  $d=4R$ . It is assumed that four truncated cylinders are free for surge mode and fixed for other modes and are studied to predict surge radiation and diffraction IRFs in time and added-mass, damping coefficients and exciting force amplitudes in frequency domain. The present ITU-WAVE numerical results for surge added-mass and damping coefficients and exciting force amplitude with heading angle  $\beta = 180^\circ$  are compared with the analytical results [10].

Fig. 13 shows surge radiation IRFs for four and single body. As four truncated vertical cylinders are symmetric, only single hull form is discretized for numerical analysis as in two truncated vertical cylinders. Numerical experience showed that numerical results at panel number 200 on single hull form is converged and used for the present ITU-WAVE numerical calculations for both four and single truncated vertical cylinder with the non-dimensional time step size of 0.05.

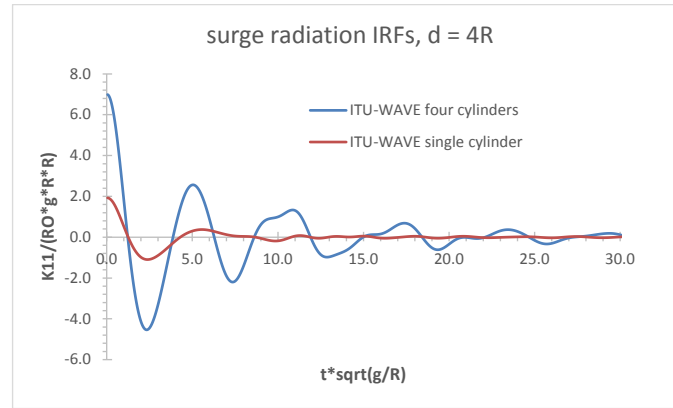


Fig. 13: Four (2x2) truncated vertical cylinders as a single mass - non-dimensional surge radiation  $K_{11}(t)$  IRFs at separation distance between body centres  $d = 4R$  and head seas  $\beta = 180^\circ$

When two (Fig. 3) and four (Fig. 13) truncated vertical cylinders' radiation IRFs are compared, it can be observed that the amplitude of radiation IRFs of four truncated cylinders are approximately 2.5 times bigger than two cylinders' radiation IRFs. Four cylinders' IRFs have also oscillations over longer times with decreasing amplitude in surge mode compared to that of two cylinders. This behaviour implicitly means that more energy captured between bodies in four cylinders than two cylinders.

It may be noticed that the magnitude of radiation IRFs of four cylinders in surge mode in Fig. 13 is more than three times of IRF of single cylinder. The other distinctive difference of IRF of four and single cylinders in Fig. 13 is the behaviour of these IRFs in longer times. IRF of four cylinders have oscillations over longer times with decreasing amplitude in surge mode while single cylinder IRF decays to zero just after first oscillation. This behaviour of IRF implicitly means that the energy between four cylinders is trapped in the gap and only a minor part of the energy is radiated outwards each time when the wave is reflected off the hull while all energy is dissipated in the case of single cylinder. It is expected that geometry of four bodies would significantly affects the radiated and trapped waves which result from due to standing waves in the gap.

Fig. 14 shows added-mass  $A_{11}(\omega)$  and damping coefficients  $B_{11}(\omega)$  which are obtained by the Fourier transform of surge radiation IRF  $K_{11}(t)$  of Fig. 13. ITU-WAVE numerical results of four cylinders are satisfactory agreement with those of [10] as can be seen in Fig. 14.

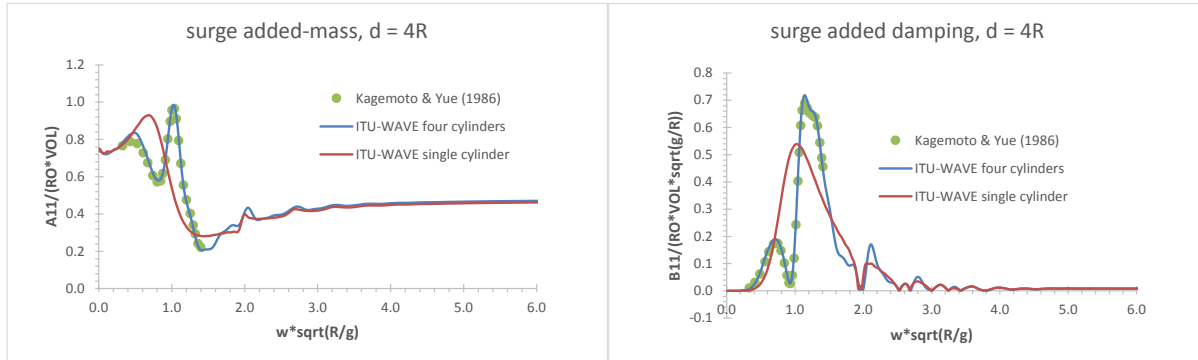


Fig. 14: Four (2x2) truncated vertical cylinders as a single mass - non-dimensional surge added-mass and damping coefficients at separation distance between body centres  $d=4R$  and head seas  $\beta = 180^\circ$ .

There would not be energy transfer or radiated waves from floating body to sea when the damping coefficients are zero as can be observed in Fig. 14. It may be noticed that there are three resonance behaviours in damping coefficients in surge mode which implies that high standing waves occur between the maximum and minimum damping coefficients [43,44]. It may be also noticed that the peaks are finite at non-dimensional resonance frequencies as some of the wave energy dissipate under the floating body and radiates to the far field.

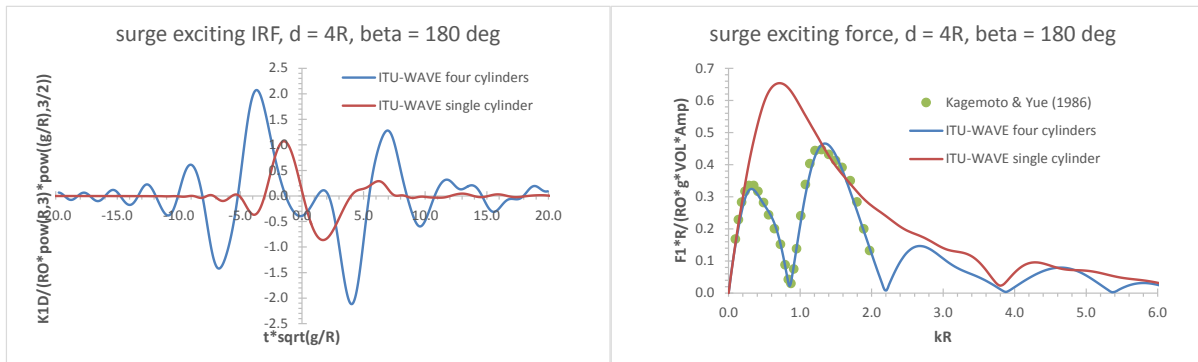


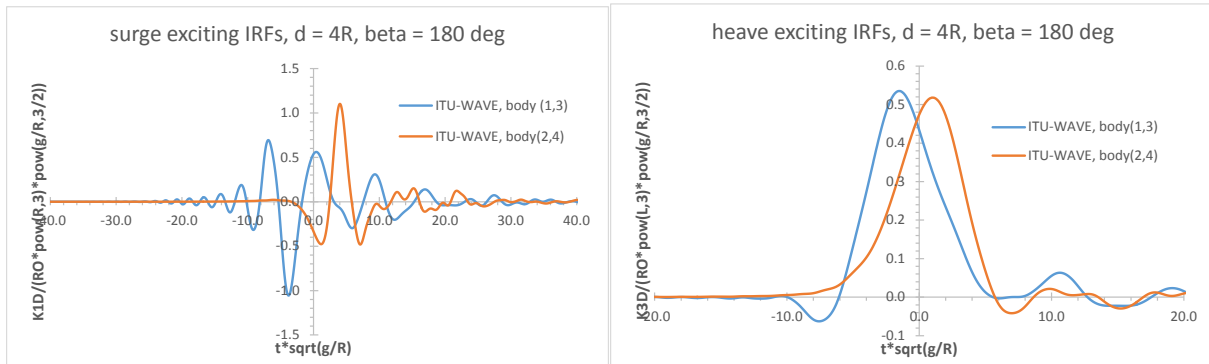
Fig. 15: Four (2x2) truncated vertical cylinders as a single mass - non-dimensional surge exciting IRFs (left) and force amplitude (right) at separation distance between body centres  $d=4R$  and head seas  $\beta = 180^\circ$ .

Fig. 15 shows surge IRFs (left) for four and single cylinders, and exciting force amplitudes  $F_1(\omega)$  (right) which are obtained by the Fourier transform of exciting surge IRF  $K_{1D}(t)$  of Fig. 15 (right). ITU-WAVE numerical results of four cylinders are satisfactory agreement with those of [10].



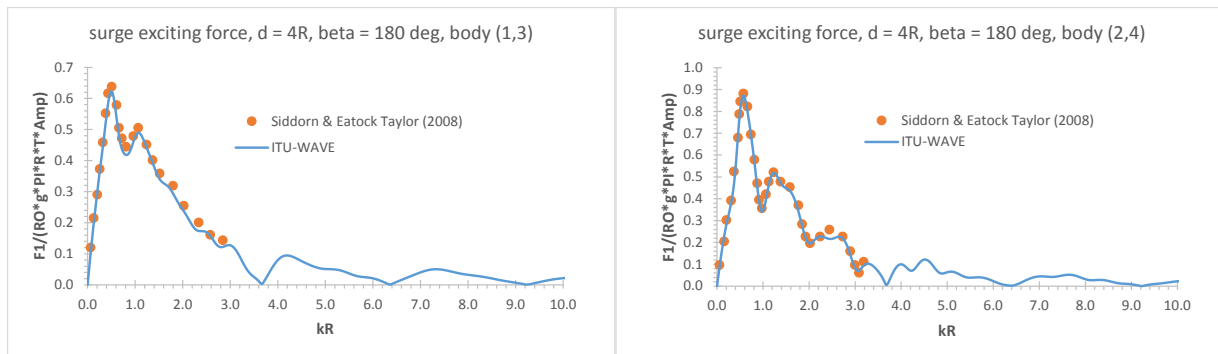
### 5.2.2. Four (2x2) truncated vertical cylinder arrays as an individual mass

As in four truncated cylinders which are considered as single unit, it is assumed that four truncated cylinders which are considered as an individual mass have the same radius  $R$  and draught  $2R$ . the separation distance between centre of the cylinders are taken as  $d = 4R$ .



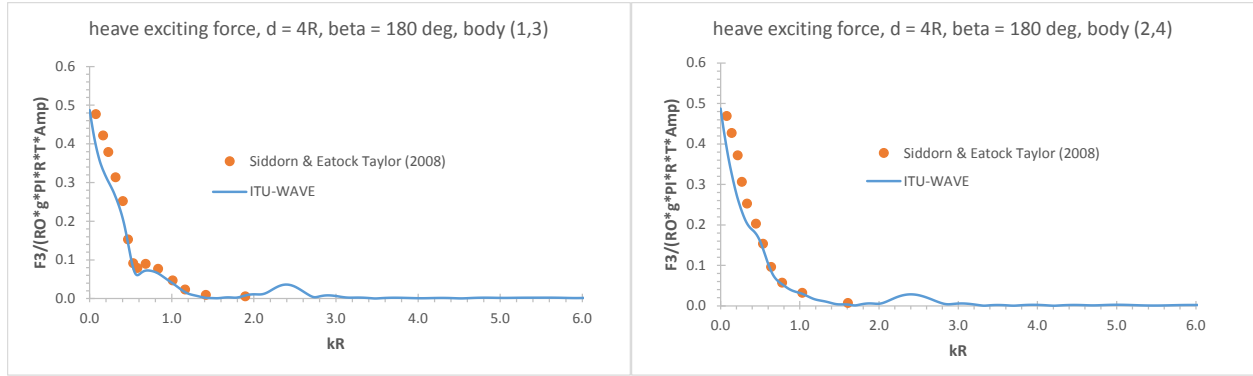
**Fig. 16:** Four (2x2) truncated vertical cylinders as an individual mass - non-dimensional exciting surge and heave IRFs at separation distance between body centres  $d=4R$ , body(1,3) represents first and third body and body(2,4) represents second and fourth body of Fig. 12.

Fig. 16 presents the non-dimensional surge (left) and heave (right) exciting IRFs, which is sum of Froude-Krylov and diffraction, at separation distance between centre of bodies  $d = 4R$  at heading angle 180 degrees. Due to symmetry, IRFs of body 1 and body 3 as well as body 2 and body 4 are the same.



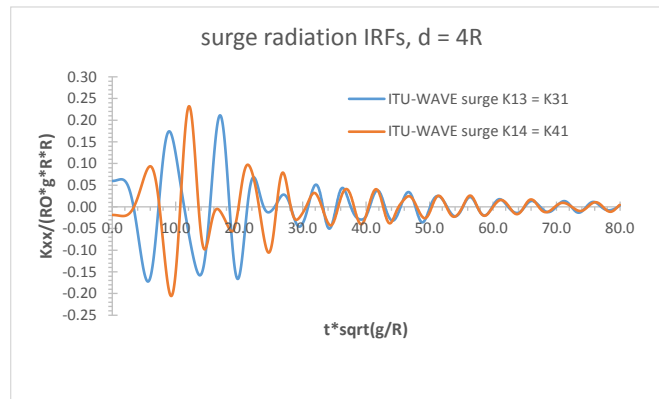
**Fig. 17:** Four (2x2) truncated vertical cylinders as an individual mass - non-dimensional exciting surge forces for body(1,3) and body(2,4) at separation distance between body centres  $d=4R$  and heading angle 180 degrees, body(1,3) represents first and third body and body(2,4) represents second and fourth body of Fig. 12.

Fig. 17 (left) shows the non-dimensional surge exciting force for body 1 and body 3 which are the same due to symmetry whilst Fig. 17 (right) is for body 2 and body 4 at separation distance  $d = 4R$  and heading angle 180 degrees. Fig. 17 is obtained by the Fourier transform of Fig. 16 (left). The present ITU-WAVE numerical results are compared with analytical results of [42] which show acceptable agreement.



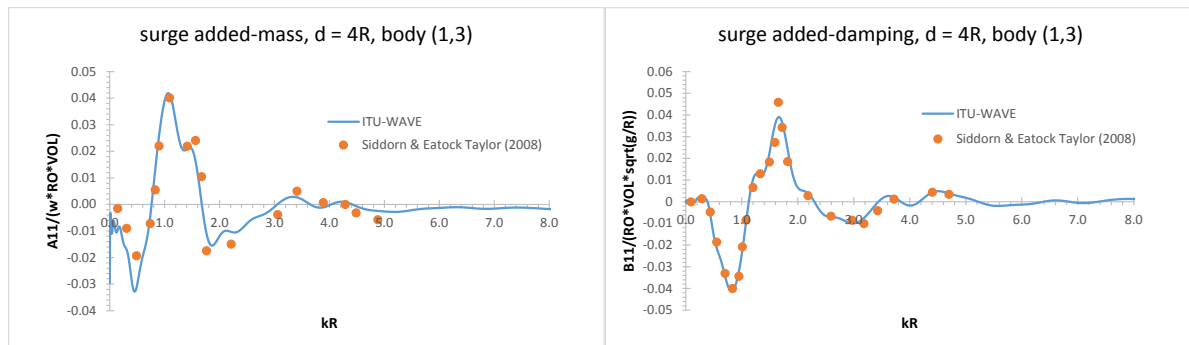
**Fig. 18:** Four (2x2) truncated vertical cylinders as an individual mass - non-dimensional exciting heave force amplitude for body(1,3) and body(2,4) at separation distance  $d = 4R$  and heading angle 180 degrees, body(1,3) represents first and third body and body(2,4) represents second and fourth body of Fig. 12.

Similar to Fig. 17, Fig. 18 shows the same results for heave mode and compared with analytical results [42] which again show acceptable agreement. Fig. 18 is obtained by the Fourier transform of Fig. 16 (right).



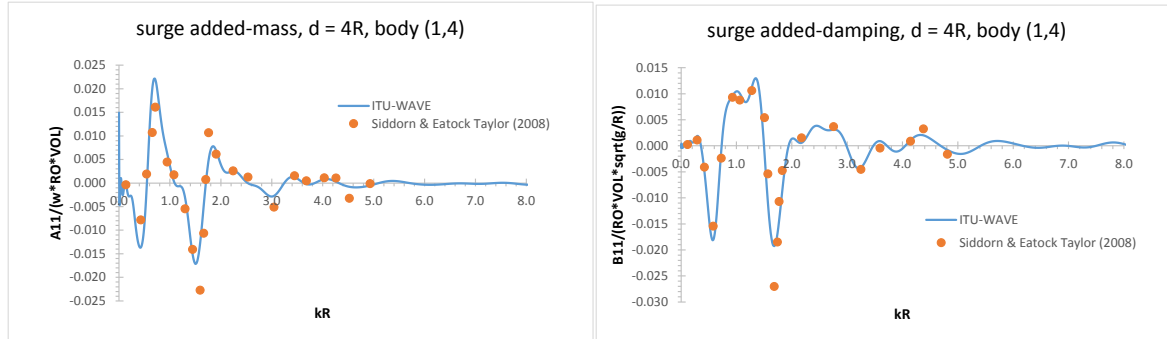
**Fig. 19:** Four (2x2) truncated vertical cylinders as an individual mass - non-dimensional radiation surge IRFs at separation distance between body centres  $d = 4R$  of Fig. 12.

Fig. 19 presents the non-dimensional surge interaction IRF K13 and K14 with a centre to centre separation distance  $d=4R$  for 2x2 array system for each multibody.



**Fig. 20:** Four (2x2) truncated vertical cylinders as an individual mass - non-dimensional radiation surge added-mass and damping coefficients at separation distance between body centres  $d = 4R$ , body(1,3) represents interaction of first and third body of Fig. 12.

Fig. 20 shows the surge mode interaction added-mass (left) and damping (right) coefficients between body 1 and body 3 at separation distance  $d = 4R$ . Fig. 20 is obtained by the Fourier transform of Fig.19. The present ITU-WAVE numerical results are compared with analytical results [42] which show acceptable agreement.

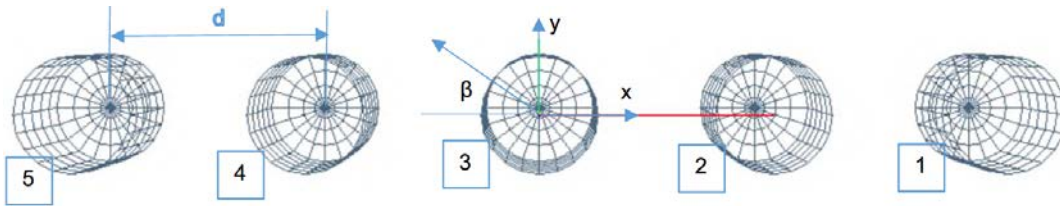


**Fig. 21:** Four (2x2) truncated vertical cylinders as an individual mass - non-dimensional radiation surge added-mass and damping coefficients at separation distance between body centres  $d = 4R$ , body(1,4) represents interaction of first and fourth body of Fig. 12.

Similar to Fig. 20, Fig. 21 shows the same interaction added-mass and damping results for body 1 and body 4 in surge mode and also compared with analytical results [42] which again also show acceptable agreement. Fig. 21 is obtained by the Fourier transform of Fig. 19.

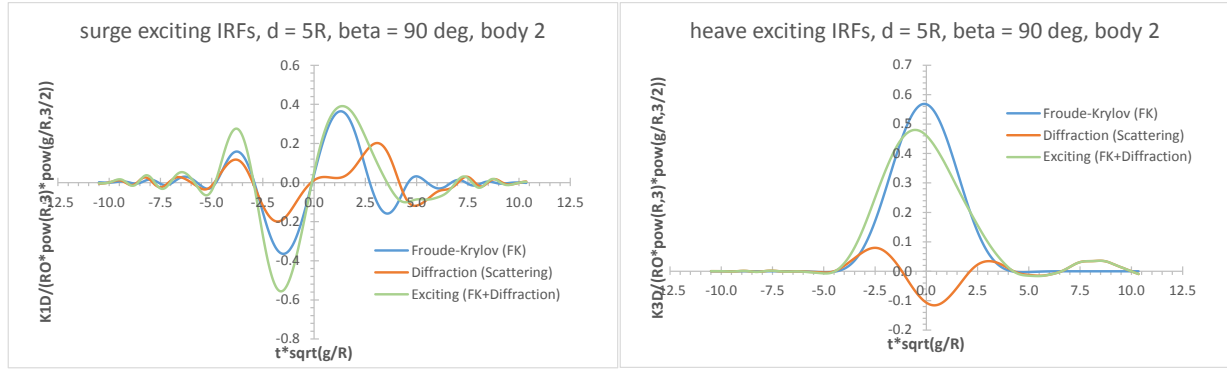
### 5.3. Five (1x5) truncated vertical cylinder arrays as an individual mass

The five truncated cylinders have the radius  $R$ , draught  $R$  and hull separation between centre of the bodies  $d=5R$ . It is assumed that five truncated cylinders are free in surge and heave mode and fixed for other modes.



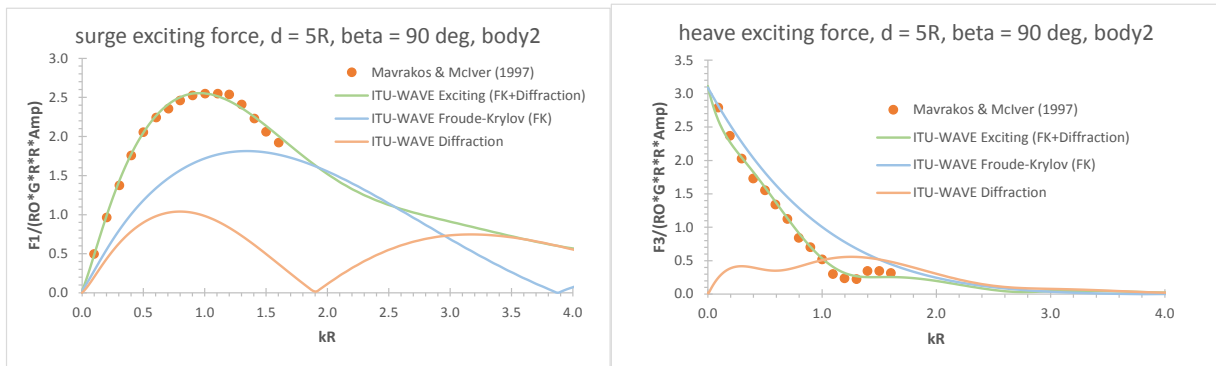
**Fig. 22:** Five (1x5) truncated vertical cylinders with hull separation distance between body centres  $d = 5R$

These five truncated cylinders are studied to predict heave radiation as well as surge and heave exciting including Froude-Krylov and diffraction (or scattering) IRFs in time domain and added-mass, damping coefficients and exciting forces in frequency domain.



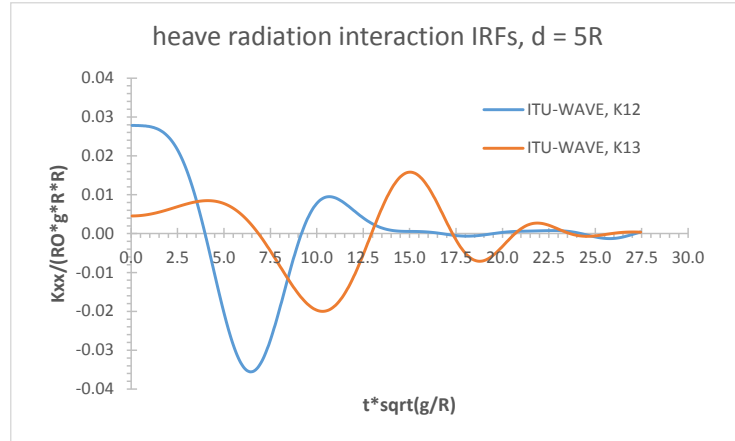
**Fig. 23:** Five (1x5) truncated vertical cylinders as an individual mass - non-dimensional surge and heave exciting IRFs with diffraction and Froude-Krylov at separation distance between body centres  $d = 5R$  of Fig. 22 and heading angle 90 degrees.

Fig. 23 shows surge and heave exciting IRFs including Froude-Krylov and diffraction at separation distance between body centres  $d = 5R$  and heading angle 90 degrees. Froude-Krylov approximation assumes that the incident wave is not diffracted which implies that force is predicted in the absence of floating multibodies and IRFs are predicted by integrating the fluid pressure on each multibody whilst the diffraction IRFs take into account the effects of the scattered waves on each multibody. It may be noticed that the contribution of Froude-Krylov IRFs in both surge and heave modes in Fig. 23 are much bigger than that of diffraction IRFs. This is mainly due to dimension of the floating bodies compared to wave length which is bigger than dimension of the present considered floating multibodies in an array system.



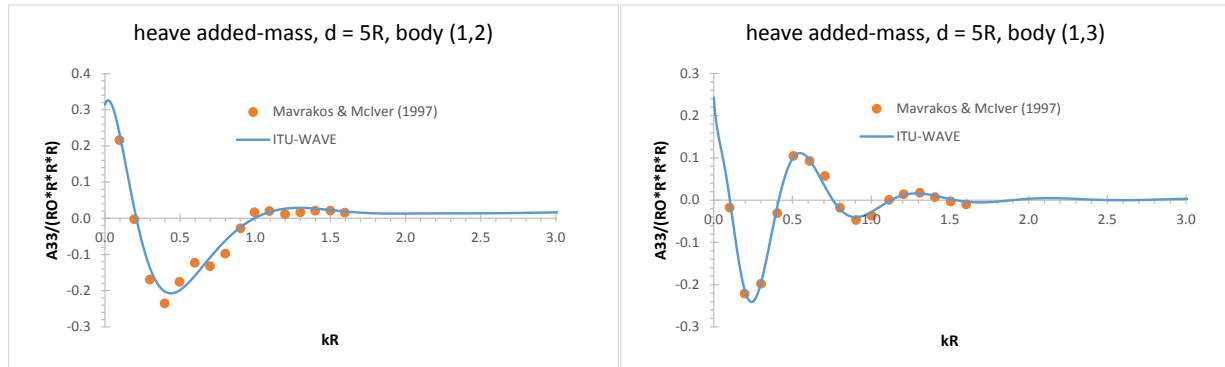
**Fig. 24:** Five (1x5) truncated vertical cylinders as an individual mass- non-dimensional exciting surge (left) and heave (right) force amplitude for body 2 of Fig. 22 at separation distance between body centres  $d = 5R$  and heading angle 90 degrees.

Fig. 24 shows non-dimensional surge and heave exciting force amplitudes with separation distance  $d = 5R$  at heading angle 90 degrees for the body 2 of Fig. 22. Fig. 24 (left) and (right) are obtained by the Fourier transform of Fig. 23 (left) and (right), respectively. The present ITU-WAVE numerical results in both surge and heave modes show very good agreement with published numerical results [45].



**Fig. 25:** Five (1x5) truncated vertical cylinders as an individual mass - non-dimensional radiation heave IRFs for the interactions of body 1 and body 2 as well as body 1 and body 3 at separation distance between body centres  $d = 5R$  of Fig. 22.

Fig. 25 shows the non-dimensional radiation interaction IRFs between body 1 and body 2 as well as body 1 and body 3 at separation distance between centre of the bodies  $d = 5R$ . It may be noticed in Fig. 25 that when the separation distance increased between bodies, the amplitude of the IFRS at lower times are decreased and oscillations are shifted larger times.



**Fig. 26:** Five (1x5) truncated vertical cylinders as an individual mass - non-dimensional radiation heave added-mass and damping coefficients at separation distance between body centres  $d = 5R$ , body(1,2) represents interaction of first and second body and body(1,3) interaction of first and third body of Fig. 22.

Fig. 26 presents non-dimensional interaction added-mass at separation distance  $d = 5R$  between body 1 and body 2 as well as body 1 and body 3. Fig. 26 is obtained by the Fourier transform of Fig. 25. The present numerical results ITU-WAVE are compared with other published numerical results [45] which show acceptable agreement. It may be noticed in Fig. 26 when the separation distance increases between bodies, the added-mass shows irregular behaviour in larger incident non-dimensional wave frequencies.

#### 5.4. Nine (1x9) truncated vertical cylinder arrays as an individual mass

The nine truncated vertical cylinders in Fig. 1 have the radius  $R$ , draught  $R/2$  and hull separation between centre of the bodies  $d = 12R$ . It is assumed that nine truncated vertical cylinders are free in heave mode and fixed for other modes. These nine truncated cylinders are studied to predict heave exciting IRFs including Froude-Krylov and diffraction Fig. 27 (left) in time and exciting forces in frequency domain Fig. 27 (right).

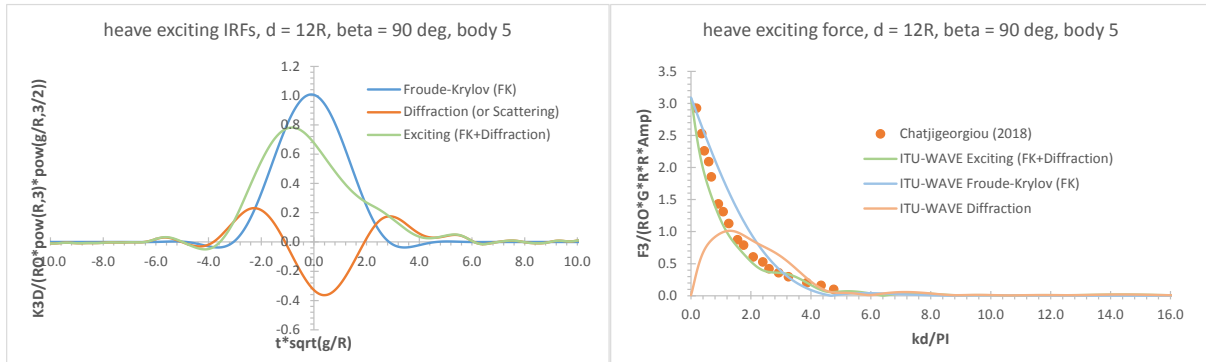


**Fig. 27:** Nine (1x9) truncated vertical cylinders as an individual mass - non-dimensional exciting IRFs (left) and heave force amplitudes for body 5 at separation distance between body centres  $d = 12R$  and heading angle 90 degrees.

Fig. 27 (left) presents non-dimensional heave IRFs at separation distance  $d = 12R$  and heading angle 90 degrees for body 5 which is the middle body in 1x9 linear array system. The contribution of Froude-Krylov IRF to total exciting IRF is much bigger than diffraction effect. This can be clearly observed in Fig. 27 (right) in the frequency domain which is the Fourier transform of Fig. 27 (left). The present ITU-WAVE exciting force frequency domain numerical result is compared with analytical result [46] which shows acceptable agreement.

### 6. Response Amplitude Operators (RAOs)

The present in-house computational code ITU-WAVE is also validated against other numerical and experimental results for the RAOs of different floating bodies in an array system including free decay motion of hemisphere, 1x2 truncated vertical cylinders and 1x5 spheroids.

#### 6.1. Free decay motion of single hemisphere

The transient free decay motion of hemisphere in heave mode is studied. The free decay motion, which can be used for the prediction of the natural frequencies of the floating bodies, implicitly means that excitation force is absent in the right-hand side of Eq. (1). The hemisphere is released from an initial displacement ( $h$ ) in heave mode at time  $t=0$  whilst the velocity of the body is zero. As the excitation force is zero, this means that free decay motion is controlled by time dependent radiation convolution integral in left-hand side of Eq. (1), which represent the memory (or transient) effect due to free surface.

The hemisphere has radius  $R = 0.254\text{m}$  and initial displacement  $h = 0.0251\text{m}$ , which are the same radius and displacement that used in experimental study that referenced in [21].

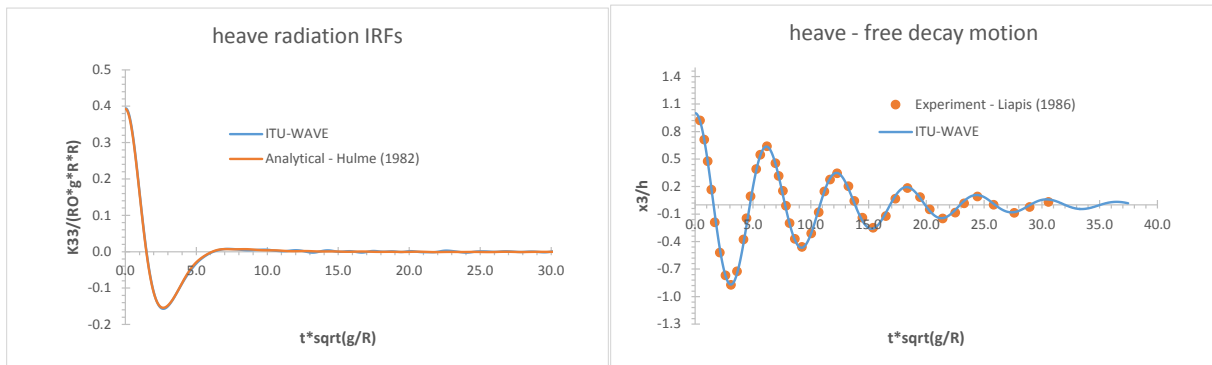


**Fig. 28:** Hemisphere radiation heave IRFs (left) and free decay motion (right) with radius  $R = 0.254\text{m}$  and initial displacement  $h = 0.0251\text{m}$ .

Fig. 28 (left) presents non-dimensional heave IRF together with analytical result [47]. As can be seen in Fig. 28 (left), the numerical and analytical results are perfectly matched. The analytical result is obtained by inverse Fourier transform by using added-damping coefficients of [47]. The free decay motion of present ITU-WAVE numerical result in heave mode is compared with experimental result that is presented in [21]. As in heave radiation IRF comparison in Fig. 28 (left), the agreement between present ITU-WAVE numerical and experimental results for free decay motion Fig. 28 (right) are perfectly matched. Fourth-order Runge-Kutta method is used for the time marching of equation of motion Eq. (1).

## 6.2. Two (1x2) truncated vertical cylinders as an individual mass

Two truncated vertical cylinders in Fig. 2 have the radius  $R$ , draught  $R/2$  with a centre to centre separation distance  $d = 5R$ . It is assumed that two truncated vertical cylinders are free in heave mode and fixed for other modes. The heave mode RAO in Fig. 29 is obtained by time marching of Eq. (1) with fourth-order Runge-Kutta method and requires the knowledge of convolution of radiation and diffraction IRFs at previous and current time steps.

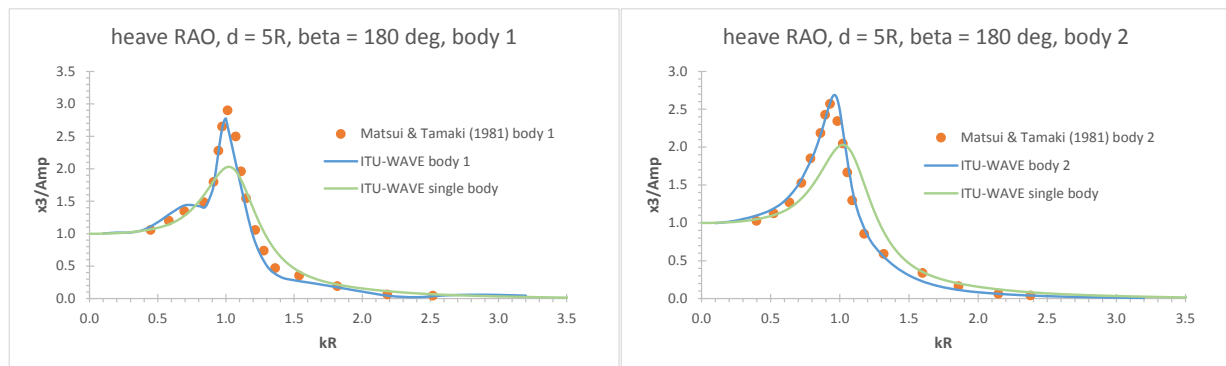
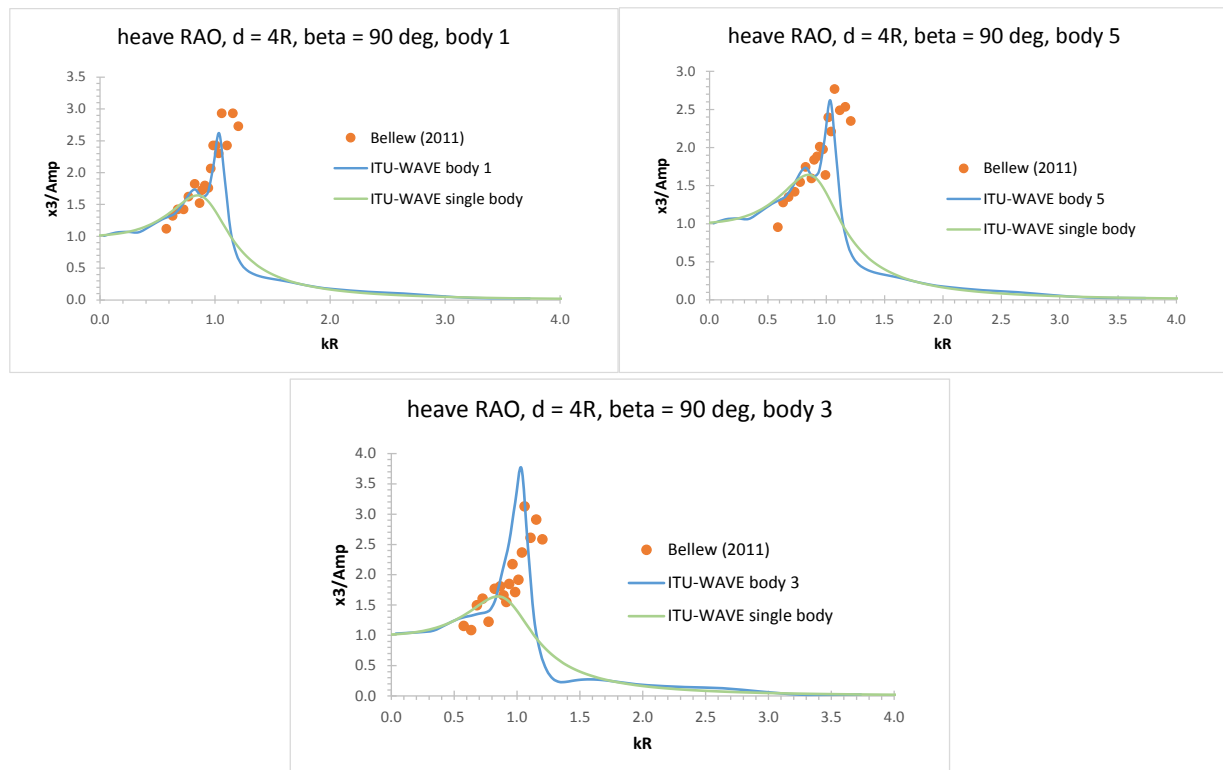


**Fig. 29:** Two (1x2) truncated vertical cylinders as an individual mass - non-dimensional heave motion RAOs at separation distance between body centres  $d = 5R$  and heading angle 180 degrees of Fig. 2.

Fig.29 shows non-dimensional heave RAO in a range of non-dimensional frequency for body 1 and body 2 at a centre to centre separation distance  $d = 5R$  and heading angle 180 degrees. The heave RAO of single body is also included in Fig. 29 for comparison purposes. The present ITU-WAVE numerical result is compared with the numerical results of [27] and shows satisfactory agreement. It may be noticed that the RAO for body 1 which meets the incident wave first is affected considerably compared to body 2 which is in the wake of body 1. This is mainly due to wave reflection effects from body 2. It may be also noticed that response amplitude of both body 1 and body 2 at around resonant frequency region is greater than single body. This is mainly due to trapped wave and standing waves in the gap of array system.

### 6.3. Five (1x5) spheroids as an individual mass

Five spheroids, which have the same linear array arrangement as in Fig. 22, have the radius  $R = 0.076\text{m}$  and draught radius  $T = 0.065\text{m}$  with a centre to centre separation distance  $d = 4R$ . It is assumed that five spheroids are free in heave mode and fixed for other modes. The heave mode RAOs on each multibody spheroids in Fig. 30 is obtained by time marching of Eq. (1).





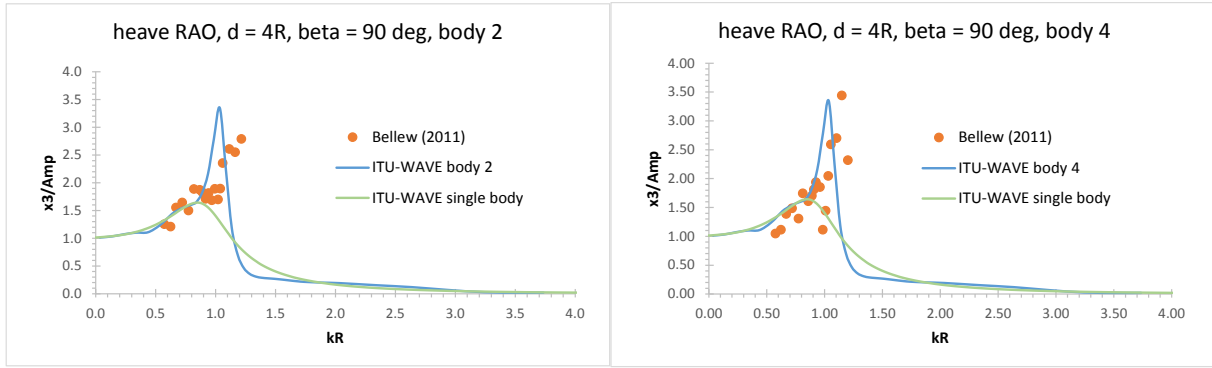


**Fig. 30:** Five (1x5) spheroids as an individual mass- non-dimensional heave motion RAOs at separation distance between body centres  $d = 4R$  and heading angle 90 degrees.

Fig. 30 presents non-dimensional RAOs of five linear spheroids for each body at separation distance between centres  $d = 4R$  and heading angle 90 degrees. It may be noticed that the present ITU-WAVE RAOs of body 1 and body 5 as well as body 2 and body 4 are the same due to symmetry. However, these symmetry relations are not present in experimental results [48] for body 2 and body 4. As it is expected body 3, which is in the middle, has greater response due to trapped waves in the gaps of body 3 whilst body 1 and body 5, which are in outer side of linear arrangement, has least response amplitude. When the present ITU-WAVE numerical predictions for RAOs are compared with experimental results [48], it can be seen that overall agreements between numerical and experimental results are satisfactory level.

## 7. Conclusions

The numerical capability and application of present in-house ITU-WAVE three-dimensional transient wave-structure interaction panel method is extended to predict the multibody interaction effects for different configuration of linear two, five and nine arrays and square arrays. The present numerical results in different modes of motion are validated with analytical, other numerical and square array results after obtaining the added-mass and damping coefficients as well as exciting force amplitude using Fourier transforms of radiation and diffraction IRFs in time domain, respectively in order to present the results in frequency domain. It is shown that the present numerical results ITU-WAVE shows satisfactory agreement with other analytical, other numerical and experimental results.

The numerical experience also shows that if the bodies in arrays are in close proximity, the multibody hydrodynamic interactions are stronger. These interaction effects are considerably diminished and shifted to larger times when the separation distances are increased. It is also shown that the RAOs of the middle body in five (1x5) linear array system has experience maximum motion amplitude compared to outer and inner bodies due to energy that trapped in the gap of array system.

## 8. Acknowledgements

The author would like to acknowledge the financial support of Royal Academy of Engineering under the UK-China Industry Academy Partnership Programme (Grant No: UK-CIAPP\73).

## 9. References

- [1] Budal K. Theory for absorption of wave power by a system of interacting bodies. *Journal of Ship Research* 1977;21(4):248-253.
- [2] Thomas GP, Evans DV. Arrays of three-dimensional wave-energy absorbers. *Journal of Fluid Mechanics* 1981;108:67-88.
- [3] McIver P, Evans DV. Approximation of wave forces on cylinder arrays. *Applied Ocean Engineering* 1984;6(2):101-107.
- [4] Simon MJ. Multiple scattering in arrays of axisymmetric wave-energy devices. Part 1. A matrix method using a plane-wave approximation. *Journal of Fluid Mechanics* 1982;120:1-25.
- [5] Spring BH, Monkmeyer PL. Interaction of plane waves with vertical cylinders. *Proceedings of 14<sup>th</sup> international conference on coastal engineering* 1974;1828-1845.
- [6] Mavrakos SA. Hydrodynamic coefficients for groups of interacting vertical axisymmetric bodies. *Ocean Engineering* 1991;18:485-515.
- [7] Ohkusu M. Wave action on groups of vertical circular cylinders. *Journal of the Society of Naval Architects in Japan* 1972;131.
- [8] Twersky V. 1952. Multiple scattering of radiation by an arbitrary configuration of parallel cylinders. *The Journal of the acoustical society of America* 1952;24 (1):42-46.
- [9] Linton CM, McIver M. *Handbook of mathematical techniques for wave-structure interactions*. Chapman and Hall 2001.
- [10] Kagemoto H, Yue DKP. Interactions among multiple three-dimensional bodies in water waves: an exact algebraic method. *Journal of Fluid Mechanics* 1986;166:189-209.
- [11] Kagemoto H, Yue DKP. Hydrodynamic interaction analyses of very large floating structures. *Marine Structures* 1993;6:295-322.
- [12] Kashiwagi M. Hydrodynamic interactions among a great number of columns supporting a very flexible structure. *Journal of Fluids and Structures* 2000;14:1013-1034.
- [13] Yilmaz O. Hydrodynamic interactions of waves with group of truncated vertical cylinders. *Journal of Waterway, Port, Coastal and Ocean Engineering* 1998;124(5):272-279.
- [14] Child B, Venugopal V. Optimal configurations of wave energy device arrays. *Ocean Engineering* 2010;37:1402-1417.
- [15] van't Veer AP, Siregar FRT. The interaction effects on a catamaran travelling with forward speed in waves. *Proceedings of 3<sup>rd</sup> International Conference of Fast Sea Transportation* 1995; 87-98.
- [16] Breit S, Sclavounos P. Wave Interaction Between Adjacent Slender Bodies. *Journal of Fluid Mechanics* 1986;165:273-296.
- [17] Kashiwagi M. Heave and Pitch Motions of a Catamaran Advancing in Waves. *Proceedings of 2<sup>nd</sup> International Conference on Fast Sea Transportations, Yokohama, Japan* 1993;643-655.
- [18] Yu YH and Li Y. Reynolds-averaged Navier–Stokes simulation of the heave performance of a two-body floating-point absorber wave energy system. *Computers & Fluids* 2013; 73: 104–114.
- [19] Kara F. Time domain hydrodynamics and hydroelastics analysis of floating bodies with forward speed. PhD thesis, University of Strathclyde, Glasgow, UK 2000.

- 760 [20] King BW. Time Domain Analysis of Wave Exciting Forces on Ships and Bodies. PhD thesis, The  
761 University of Michigan, Ann Arbor, Michigan, USA 1987.
- 762 [21] Liapis S. Time Domain Analysis of Ship Motions. PhD thesis, The University of Michigan, Ann  
763 Arbor, Michigan, USA 1986.
- 764 [22] Bertram V. Ship Motions by Rankine Source Method. Ship Technology Research 1990;37 (4):143-  
765 152.
- 766 [23] Nakos D, Kring D, Sclavounos PD. Rankine Panel Method for Transient Free Surface Flows.  
767 Proceedings of the 6<sup>th</sup> International Symposium on Numerical Hydrodynamics, Iowa City, I.A.,  
768 USA 1993;613-632.
- 769 [24] Xiang X, Faltinsen OM. Time domain simulation of two interacting ships advancing parallel in  
770 waves. Proceedings of the ASME 30<sup>th</sup> International Conference on Ocean, Offshore and Arctic  
771 Engineering, Rotherdam, The Netherlands 2011.
- 772 [25] Maniar HD, Newman JN. Wave diffraction by a long array of cylinders. Journal of Fluid  
773 Mechanics 1997;339:309-330.
- 774 [26] Chakrabarti SK. Hydrodynamic interaction forces on multi-moduled structures. Ocean  
775 Engineering 2000;27:1037-1063.
- 776 [27] Matsui T, Tamaki T. Hydrodynamic interaction between groups of vertical axisymmetric bodies  
777 floating in waves. Proceedings of International Symposium on Hydrodynamics in Ocean  
778 Engineering 1981;817-836.
- 779 [28] Wolgamot HA, Eatock Taylor R, Taylor PH. Radiation, trapping and near trapping in arrays of  
780 floating truncated cylinders. Journal of Engineering Mathematics 2015;91:17-35.
- 781 [29] Kara F. Time domain prediction of power absorption from ocean waves with wave energy  
782 converters arrays. Renewable Energy 2016;92:30-46.
- 783 [30] Kara F. Wave energy converter arrays for electricity generation with time domain analysis. In  
784 Offshore Mechatronics Systems Engineering 2018;Chapter 6:131-160.
- 785 [31] Kara F. Time domain prediction of seakeeping behaviour of catamarans. International  
786 Shipbuilding Progress 2016;62(3-4):161-187.
- 787 [32] Kara F. Time domain prediction of hydroelasticity of floating bodies. Applied Ocean Research  
788 2015;51:1-13.
- 789 [33] Kara F. Time domain prediction of added-resistance of ships. Journal of Ship Research 2011;55  
790 (3):163-184.
- 791 [34] Kara F. Time domain prediction of power absorption from ocean waves with latching control.  
792 Renewable Energy 2010;35:423-434.
- 793 [35] Kara F, Vassalos D. Hydroelastic analysis of cantilever plate in time domain. Ocean Engineering  
794 2007;34:122-132.
- 795 [36] Kara F, Vassalos D. Time domain computation of wavemaking resistance of ships. Journal of Ship  
796 Research 2005;49 (2):144-158.
- 797 [37] Kara F, Vassalos D. Time domain prediction of steady and unsteady marine hydrodynamic  
798 problem. International Shipbuilding Progress 2003;50(4):317-332.
- 799 [38] Cummins WE. The Impulse response function and ship motions. Schiffstechnik 1962;9:101-109.

- [39] Ogilvie TF. Recent progress toward the understanding and prediction of ship motions. Proceedings of the 5<sup>th</sup> Symposium on Naval Hydrodynamics, Office of Naval Research, Washington, D.C., USA 1964;3-128.
- [40] Wehausen JV, Laitone EV. Surface Waves in Fluid Dynamics III in Handbuch der Physik 1960; Chapter 3:446-778
- [41] Hess JL, Smith AMO. Calculation of non-lifting potential flow about arbitrary three-dimensional bodies. Journal of Ship Research 1964;8:22-44.
- [42] Siddorn P, Eatock Taylor R. Diffraction and independent radiation by an array of floating cylinders. Ocean Engineering 2008;35:1289-1303.
- [43] Ohkusu M. On the heaving motion of two circular cylinders on the surface of a fluid. Reports of Research Institute for Applied Mechanics, No.58, 1969;17:167-185
- [44] van Oortmerssen G. Hydrodynamic interaction between two structures floating in waves. Proceedings of the 2<sup>nd</sup> International Conference on Behaviour of Offshore Structures (BOSS'79), London, UK 1979;339-356.
- [45] Mavrakos SA, McIver P. Comparison of methods for computing hydrodynamic characteristics of array of wave power devices. Applied Ocean Research 1997;19:283-291.
- [46] Chatjigeorgiou IK. Water wave trapping in a long array of bottomless circular cylinders. Wave Motion 2018;83:25-48.
- [47] Hulme A. The wave forces acting on a floating hemisphere undergoing forced periodic oscillations. Journal of Fluid Mechanics 1982;121:443-463.
- [48] Bellew S. Investigation of the response of groups of wave energy devices. PhD thesis, The University of Manchester, UK 2011.